LoS, Non-LoS and Quasi-LoS Signal Propagation: A Three State Channel Model

Jonathan W. Browning[1], Simon L. Cotton[1], Paschalis C. Sofotasios[2,3], David Morales-Jimenez[4], and Michel D. Yacoub[5]

[1]Centre for Wireless Innovation, ECIT Institute, Queen's University Belfast, Belfast, BT3 9DT, UK
[2]Centre for Cyber-Physical Systems, Department of Electrical Engineering and Computer Science, Khalifa University, Abu Dhabi 127788, UAE
[3]Department of Electrical Engineering, Tampere University, Tampere 33101, Finland
[4]Departmento de Ingenieria de Comunicaciones, Universidad de Málaga, 29071 Málaga, Spain
[5]School of Electrical and Computer Engineering, University of Campinas, Campinas 13083-970, Brazil
e-mails: {jbrowning01; simon.cotton}@qub.ac.uk, p.sofotasios@ieee.org, morales@ic.uma.es, mdyacoub@unicamp.br

***Abstract*—The modeling of wireless communications channels is often broken down into two distinct states, defined according to the optical viewpoints of the transmitter (TX) and receiver (RX) antennas, namely line-of-sight (LoS) and non-LoS (NLoS). Movement by the TX, RX, both and/or objects in the surrounding environment means that channel conditions may transition between LoS and NLoS leading to a third state of signal propagation, namely quasi-LoS (QLoS). Unfortunately, this state is largely ignored in the analysis of signal propagation in wireless channels. We therefore propose a new statistical framework that unifies signal propagation for LoS, NLoS, and QLoS channel conditions, leading to the creation of the Three State Model (TSM). The TSM has a strong physical motivation, whereby the signal propagation mechanisms underlying each state are considered to be similar to those responsible for Rician fading. However, in the TSM, the dominant signal component, if present, can be subject to shadowing. To support the use of the TSM, we develop novel formulations for the probability density functions of the in-phase and quadrature components of the complex received signal as well of the received signal envelope. The offered results are corroborated with results from respective computer simulations, whilst it is shown that the proposed model is more versatile than existing conventional models.**

I. Introduction

SIGNAL propagation in wireless channels is often assumed to take place through one of four physical mechanisms, namely line-of-sight (LoS) propagation (or free space propagation), reflection, diffraction, and scattering [1]. Determining how these mechanisms interact and contribute to the overall signal reception is non-trivial. In practice, it depends on a number of factors including the geometrical configuration of the transmitter (TX) and receiver (RX) relative to one another, the characteristics of the operating environment, the presence of blocking and scattering objects, and the frequency of operation, to name but a few. Also, LoS propagation and specular reflection tend to be the dominant processes in terms of the overall power contribution [1], while diffraction and especially scattering are critical for supporting communications in non-LoS (NLoS) scenarios where there may be no dominant signal path between the TX and RX [2]. In many practical wireless applications, the transition between LoS and NLoS channel conditions is rarely discrete and involves a third state referred to as quasi-LoS (QLoS) [3], obstructed LoS [4]–[6] or near LoS [7], [8]. In this transitory phase, there may be a reconstitution of the weighting of each of the propagation mechanisms listed above as the channel moves from LoS to NLoS and vice versa. For example, by moving from LoS, through QLoS to NLoS, a reduction in the power contributed by the dominant component can be expected (through shadowing), meaning that the link will become increasingly reliant on the mechanisms associated with NLoS propagation. Furthermore, new contributing signal components and changes in the direction of arrival (DoA) may emerge as the geometrical propagation paths evolve.

The signal propagation picture described above is a complicated one, even for each of the three states individually. Acknowledging this, it is therefore unsurprising that researchers tend to favor the use of statistical models [2], [9], [10] as opposed to analytical models [11]–[13], which become difficult to use beyond the simplest scenarios. The most commonly adopted models for LoS and NLoS propagation are the Rician [9] and Rayleigh [2] fading models, respectively [14]. Nonetheless, for many emergent applications, this may lead to an oversimplification of the signal propagation problem. As a consequence, the realistic evaluation of the performance of wireless communication systems with stringent quality of service requirements becomes detrimentally problematic.

It has been observed through field measurements that the complicated nature of propagation in applications such as in-body area networks [15]–[17], device-to-device communications [17], [18], vehicle-to-vehicle communications [19], [20], and unmanned aerial vehicle communications [21], [22] can lead to multimodal behavior in their first-order statistics. Yet, unfortunately, neither the Rayleigh nor Rician fading models, in their native form, offer the flexibility to encapsulate the transitionary behavior of the channel statistics observed in

these use cases. In this context, a recently proposed amplitude fading model that can encapsulate bimodal behavior in the statistics of the channel model is the fluctuating two-ray model [23], which considers two shadowed specular components and a scattered signal component. Another model which is bimodal in nature, is the alternate Rician shadowed (ARS) fading model [24], which uses a mixture of two shadowed Rician distributions to represent LoS and NLoS propagation conditions, whereby the shadowing remains constant across both. Although it was shown to provide a good fit to empirical data, the assumption that shadowing will be constant across both LoS and NLoS states, does not seem intuitive for most practical scenarios. Markov processes have also been utilized to model wireless communications experiencing transitionary behavior, such as the Gilbert-Elliott (GE) model [25], [26]. The GE model is comprised of a two-state Markov process and has been used to characterise burst-noise channels [25], [26]. However, using a two-state Markov process has limitations, for instance when the received signal experiences dramatic changes [27], [28]. As an extension, the finite-state Markov channel (FSMC) model was proposed [27] and later used to model Rayleigh faded channels [28]. Application of the FSMC model is non-trivial and is hampered by the fact that this model only considers Rayleigh faded states. This means that it will be unsuitable for representing the more intricate fading conditions that may arise in many emergent wireless applications, such as those considered in the present analysis.

Notably, the characteristics of the received signal envelope reveal only part of the overall channel picture since of critical importance are also the statistics of the received signal phase and those of the in-phase and quadrature components of the complex received signal. Based on this, in this paper we make significant contributions towards a unified model for short-term fading[1] in LoS, QLoS and NLoS signal propagation scenarios. To the best of our knowledge a single amalgamated model which encompasses these three channel states has yet to be proposed in the open literature. Herein, we refer to this novel fading model as the Three State Model (TSM). Within each state of the TSM, the dominant component can be perturbed by shadowing, as realistic communication scenarios dictate. Also, anisotropic filtering of the scattered signal contribution is accounted for through the TSM's second-order statistics where the direction of departure (DoD) and DoA are modeled using the Von Mises distribution [29]. Additionally, movement of the TX, RX or both is also considered in the construction of the model. To promote the use of the TSM, we develop many of its fundamental statistics including the probability density functions (PDFs) of the in-phase and quadrature components as well as the received signal envelope. It is worth mentioning that although at first glance, some of the expressions obtained for some of the fundamental statistics may appear arduous, a key feature of the TSM is that it is completely defined in terms of underlying Gaussian random variables (RVs), meaning that unlike many other comparable models, it has a strong physical motivation, and its simulation is relatively straightforward.

[1]Or equivalently small-scale fading if considering distance instead of time.

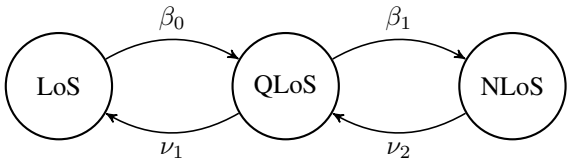

Fig. 1: The state-transition-rate diagram of the TSM.

II. Physical Model and Analytical Formulation

The TSM characterizes scenarios where a fading channel may transition between three states, namely LoS, QLoS, or NLoS. Each state has an associated probability of occurrence, p_ι, such that $\sum_{\iota\in\{L,Q,N\}} p_\iota = 1$, where the elements in ι represent a state according to L = LoS, Q = QLoS, and N = NLoS. The transitions between the three states within the TSM can be modeled using a Markov process. The transition from one state to the next corresponds to a change in the state of the (direct) optical signal path between the TX and RX. As depicted in the state-transition-rate diagram of Fig. 1, the transition rate from the LoS state to the QLoS state and back again is β_0 and ν_1, respectively. Likewise, the transition rate from the QLoS state to the NLoS state and back is β_1 and ν_2, respectively. Following from this, we may define the ratios, $A_0 = \beta_0/\nu_1$ and $A_1 = \beta_1/\nu_2$, with both A_0 and A_1 being positive real numbers. This then allows us to write the probability of occurrence of each of the three states as [30]: $p_L = [1 + A_0 + A_0A_1]^{-1}$, $p_Q = p_LA_0$, and $p_N = p_LA_0A_1$. In addition to these mathematical relationships between the transition rates and steady state probabilities, it is convenient to establish some qualitative links between them. Letting S_0, S_1 and S_2 represent the LoS, QLoS, and NLoS respectively, then for $A_i = 1$, the states S_i and S_{i+1} are equally likely. For $A_i > 1$, S_{i+1} is more likely than S_i, and otherwise for $A_i < 1$. The QLoS state can be interpreted as a transitionary state, where the geometry, and hence statistics of the channel are not fully described by either LoS or NLoS.

Since only one of the three states may occur at a time, $\mathcal{S} = R_\iota \exp(j\Theta_\iota)$ represents the complex signal envelope at a particular instance, where R_ι is the received signal envelope and Θ_ι is the phase of an individual state. In many signal propagation scenarios, especially in short range applications the geometry of the propagation problem is such that dominant signal paths may exist even in what would be considered a NLoS channel (e.g., via a strong specular reflection from a smooth wall or similar surface). In such scenarios, any dominant component which may be present could be subjected to shadowing. Any shadowing affecting the dominant component in each state is described through an independent shadowing process, causing the dominant component to fluctuate. Letting X_ι and Y_ι represent the in-phase and quadrature components of a state respectively, it follows that $\mathcal{S} = X_\iota + jY_\iota$, $R_\iota^2 = X_\iota^2 + Y_\iota^2$, $\Theta_\iota = \arg(X_\iota + jY_\iota)$, $X_\iota = R_\iota \cos(\Theta_\iota)$, $Y_\iota = R_\iota \sin(\Theta_\iota)$. Thus, the received signal power of each state, can then be modeled as

$$R_\iota^2 = (C_{sca-i,\iota} + \zeta_\iota C_{dom-i,\iota})^2 + (C_{sca-q,\iota} + \zeta_\iota C_{dom-q,\iota})^2, \quad (1)$$

where $C_{sca-i,\iota}$ and $C_{sca-q,\iota}$ are mutually independent Gaussian random processes with $\mathbb{E}[C_{sca-i,\iota}] = \mathbb{E}[C_{sca-q,\iota}] = 0$, $\mathbb{E}[C^2_{sca-i,\iota}] = \mathbb{E}[C^2_{sca-q,\iota}] = \sigma^2_\iota$, where $\mathbb{E}[\cdot]$ denotes statistical expectation. $C_{dom-i,\iota}$ and $C_{dom-q,\iota}$ represent the time-varying amplitudes of the in-phase and quadrature components of the dominant signal respectively, with the variation related to the embedded Doppler effect [31], and ζ_ι models the fluctuations of the dominant component. The Rician k factor of each state represents the ratio between the total power of the dominant component, $\delta^2_\iota = C^2_{dom-i,\iota} + C^2_{dom-q,\iota}$, and the total power of the scattered components $2\sigma^2_\iota$, with

$$2\sigma^2_\iota = \frac{\bar{r}^2_\iota}{1+k_\iota}, \tag{2}$$

where $\bar{r}_\iota = \sqrt{\mathbb{E}[R^2_\iota]}$, that is $k_\iota = (C^2_{dom-i,\iota} + C^2_{dom-q,\iota})/(2\sigma^2_\iota)$. By also defining $\varpi_\iota = \arg(C_{dom-i,\iota} + jC_{dom-q,\iota})$ as a phase parameter, we can write

$$C_{dom-i,\iota} = \sqrt{\frac{k_\iota}{1+k_\iota}}\bar{r}_\iota \cos(\varpi_\iota), \tag{3}$$

$$C_{dom-q,\iota} = \sqrt{\frac{k_\iota}{1+k_\iota}}\bar{r}_\iota \sin(\varpi_\iota). \tag{4}$$

The normalized term, ζ_ι, simultaneously impacts both the in-phase and quadrature components. It accounts for any fluctuations of the dominant component in each individual state caused by shadowing, and follows a normalized Rician distribution with PDF given by [32, eq. (2.62)], namely

$$f_{\zeta_\iota}(\zeta_\iota) = \frac{2\zeta_\iota\,(1+k_{S_\iota})\exp\left(-k_{S_\iota}\right)}{\exp\left(\zeta^2_\iota\,(1+k_{S_\iota})\right)} I_0\left(2\zeta_\iota\sqrt{k_{S_\iota}\,(1+k_{S_\iota})}\right), \tag{5}$$

where $I_0(\cdot)$ denotes the modified Bessel function of the first kind with order zero [33, eq. (8.447.1)] and $\mathbb{E}[\zeta^2_\iota] = 1$. The parameter k_{S_ι} controls the severity of the shadowing of the dominant component, with $k_{S_\iota} \to 0$, indicating severe shadowing whereas the shadowing vanishes as $k_{S_\iota} \to \infty$.

III. Three State Model Statistics

In what follows, we derive the distribution of the in-phase and quadrature components of the complex received signal and the distribution of the received signal envelope.

A. Distribution of the In-phase and Quadrature Components

Let either $Z_\iota = X_\iota$, & $\lambda_\iota = C_{dom-i,\iota}$ or $Z_\iota = Y_\iota$ & $\lambda_\iota = C_{dom-q,\iota}$, as required to represent either the in-phase or quadrature components of the complex received signal, respectively. The model presented in (1) implies that when Z_ι is conditioned on ζ_ι, it follows a Gaussian distribution [34, eq. (2.3-8)]. To find the PDF of the in-phase or quadrature components for each of the individual states, ζ_ι is averaged over in the conditioned Z_ι, similar to [35], yielding

$$f_{Z_\iota}(z_\iota) = \sqrt{\frac{1+k_\iota}{\pi\ \bar{r}^2_\iota}} \int_0^\infty \frac{f_{\zeta_\iota}(\zeta_\iota)}{\exp\left(\frac{(z_\iota-\zeta_\iota\lambda_\iota)^2(1+k_\iota)}{\bar{r}^2_\iota}\right)}\ d\zeta_\iota. \tag{6}$$

The integral in (6) can be solved by substituting (5) into (6), along with [33, eq. (8.447.1)], and applying the identities [33, eq. (3.462.1)] and [33, eq. (9.240)] sequentially to give (7), where $\eta_\iota = \bar{r}^2_\iota(1+k_{S_\iota}) + \lambda^2_\iota(1+k_\iota)$, with $\Gamma(\cdot)$ denoting the gamma function [36, eq. (06.05.02.0001.01)], and ${}_1F_1(\cdot;\cdot;\cdot)$ the confluent hypergeometric function [33, eq. (9.210.1)].

From the physical model of the TSM it is clear that the associated TSM first-order statistics are a combination of the three individual state first-order statistics in proportion with their probability of occurrence (i.e., p_L, p_Q and p_N). Now letting $\bar{r}_g = \sqrt{\mathbb{E}[R^2]}$, where $\bar{r}_g = \sum_{\iota\in\{L,Q,N\}} p_\iota \bar{r}_\iota$ and using a transformation of variables ($z_\iota = z/\bar{r}_g$), the PDF of the in-phase or quadrature components of the TSM is $f_Z(z) = \bar{r}_g \sum_{\iota\in\{L,Q,N\}} p_\iota f_{Z_\iota}(z \times \bar{r}_g)$, where $f_{Z_\iota}(\cdot)$ denotes the PDF of the in-phase or quadrature components for the relevant state as presented in (7). The PDFs of the in-phase and quadrature component are re-normalized to $\bar{r}_g$, the overall rms signal level, to ensure Z has unit power. In order to corroborate our new expressions, Monte Carlo simulations have been carried out by generating 10^7 samples of each of the underlying random processes, $C_{sca-i,\iota}$, $C_{sca-q,\iota}$, and ζ_ι and evaluating (1).

A closed-form solution to (7) is found by taking (7), then using the primary definition of the confluent hypergeometric function [36, eq. (07.20.02.0001.01)], and [36, eq. (06.10.27.0001.01)], along with the definitions [37, eq. (1.3.22)], and [37, eq. (1.3.28)] provides (8), where $F^{\vdots;\cdot}_{\vdots;\cdot}\left(\begin{smallmatrix}\cdot & \cdot & \cdot & \cdot & \cdot\\ \cdot & \cdot & \cdot & \cdot & \cdot\end{smallmatrix};\cdot,\cdot\right)$ denotes the generalized Kampé de Fériet function [37, eq. (1.3.28)] and $\Psi_2(\cdot;\cdot,\cdot;\cdot,\cdot)$ is the confluent Appell function [37, eq. (1.3.22)].

B. Distribution of the Received Signal Envelope

Following the mathematical model for the individual states of the TSM given in (1), the PDF of the received signal envelope, R_ι, can be expressed as [38, Appendix A]

$$f_{R_\iota}(r_\iota) = \frac{r_\iota}{\sigma^2_\iota \exp\left(\frac{r^2_\iota}{2\sigma^2_\iota}\right)} \int_0^\infty \frac{I_0\left(\frac{\zeta_\iota\delta_\iota r_\iota}{\sigma^2_\iota}\right)}{\exp\left(\frac{\zeta^2_\iota\delta^2_\iota}{2\sigma^2_\iota}\right)} f_{\zeta_\iota}(\zeta_\iota)\ d\zeta_\iota. \tag{9}$$

The integral in (9) can be solved by substituting (5), and using [33, eq. (8.447.1)], along with the necessary transformation of variables, and the identities [33, eq. (6.643.2)] and [33, eq. (9.220.2)]. Based on this and knowing (2) and $\delta^2_\iota = 2\sigma^2_\iota k_\iota$, (10) is obtained.

The PDF of the received signal envelope in each state, R_ι, is found to be

$$\begin{aligned} f_{R_\iota}(r_\iota) = \sum_{i=0}^{\infty} &\frac{2r^{1+2i}_\iota k^i_\iota (1+k_\iota)^{1+i}\mu_\iota \exp\left(-k_{S_\iota}\right)}{i!\bar{r}^{2(1+i)}_\iota (1+k_\iota+k_{S_\iota})^i} \\ &\times \exp\left(-\frac{r^2_\iota(1+k_\iota)}{\bar{r}^2_\iota}\right) {}_1F_1\left(1+i;1;k_{S_\iota}\mu_\iota\right), \end{aligned} \tag{10}$$

where $\mu_\iota = (1+k_{S_\iota})\,/\,(1+k_\iota+k_{S_\iota})$. Notably, as $k_{S_\iota} \to \infty$, (i.e., as the impact of shadowing on the dominant components vanishes), the PDF given in (10) approaches that of the Rician distribution. Secondly, when $k_{S_\iota} \to 0$ or $k_\iota = 0$, (10) reduces to the Rayleigh PDF.

Using a transformation of variables ($r_\iota = r/\bar{r}_g$), the PDF of the received signal envelope of the TSM is shown to be

$$f_R(r) = \bar{r}_g \sum_{\iota\in\{L,Q,N\}} p_\iota f_{R_\iota}(r \times \bar{r}_g), \tag{11}$$

$$f_{Z_\iota}(z_\iota) = \sum_{i=0}^{\infty} \frac{\sqrt{1+k_\iota}\,(1+k_{S_\iota})^{1+i}\, k_{S_\iota}^{i} \bar{r}_\iota^{2i} \exp\left(-k_{S_\iota}\right)}{\sqrt{\pi}\eta_\iota^{\frac{3}{2}+i}\Gamma(1+i)i! \exp\left(\frac{z_\iota^2(1+k_\iota)}{\bar{r}_\iota^2}\right)} \left[\bar{r}_\iota \Gamma\left(1+i\right)\sqrt{\eta_\iota}\, {}_1F_1\left(1+i; \frac{1}{2}; \frac{\left(z_\iota\lambda_\iota(1+k_\iota)\right)^2}{\bar{r}_\iota^2\eta_\iota}\right) + 2z_\iota\lambda_\iota(1+k_\iota)\Gamma\left(\frac{3}{2}+i\right) {}_1F_1\left(\frac{3}{2}+i; \frac{3}{2}; \frac{\left(z_\iota\lambda_\iota(1+k_\iota)\right)^2}{\bar{r}_\iota^2\eta_\iota}\right)\right]. \tag{7}$$

$$f_{Z_\iota}(z_\iota) = \frac{\sqrt{1+k_\iota}\,(1+k_{S_\iota})}{\sqrt{\pi}\eta_\iota} \exp\left(-k_{S_\iota} - \frac{z_\iota^2(1+k_\iota)}{\bar{r}_\iota^2}\right) \left[\frac{2z_\iota\lambda_\iota\left(1+k_\iota\right)}{\sqrt{\eta_\iota}} \times \Psi_2\left(\frac{3}{2}; \frac{3}{2}, 1; \frac{\left(z_\iota\lambda_\iota(1+k_\iota)\right)^2}{\bar{r}_\iota^2\eta_\iota}, \frac{\bar{r}_\iota^2 k_{S_\iota}(1+k_{S_\iota})}{\eta_\iota}\right) + \bar{r}_\iota F_{0:1;0}^{1:0;0}\left(\begin{matrix}1:-;-;\\ -:\frac{1}{2};-;\end{matrix} \frac{\left(z_\iota\lambda_\iota(1+k_\iota)\right)^2}{\bar{r}_\iota^2\eta_\iota}, \frac{\bar{r}_\iota^2 k_{S_\iota}(1+k_{S_\iota})}{\eta_\iota}\right)\right]. \tag{8}$$

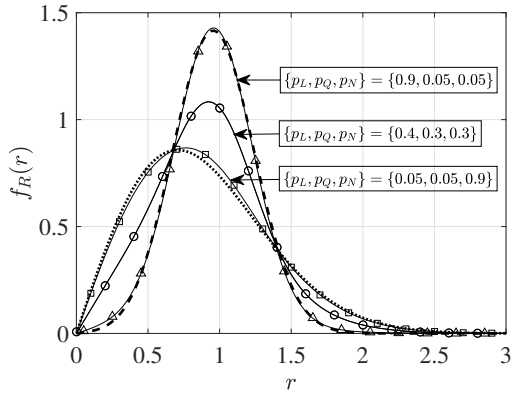

Fig. 2: The PDF of the TSM received signal envelope (lines) and corresponding simulation results (shapes) are shown for p_ι varying. The Rician PDF (dashed line) is shown for $K = 5$, $\bar{r} = 1$, and the Rayleigh PDF (dotted line) is shown for $\bar{r} = 1$.

where $f_{R_\iota}(\cdot)$ represents the PDF of the received signal envelope for each of the individual states as given in (10). The PDF of the received signal envelope is re-normalized to the overall rms signal level to ensure R has unit power.

By using [36, eq. (07.20.02.0001.01)] and the identities [36, eq. (06.10.27.0001.01)] and [37, eq. (1.3.22)] in (10), a closed-form solution for the PDF of the received signal envelope in each state is found to be

$$f_{R_\iota}(r_\iota) = \frac{2r_\iota(1+k_\iota)\mu_\iota}{\bar{r}_\iota^2} \exp\left(-k_{S_\iota} - \frac{r_\iota^2(1+k_\iota)}{\bar{r}_\iota^2}\right) \times \Psi_2\left(1; 1, 1; \frac{r_\iota^2 k_\iota(1+k_\iota)}{\bar{r}_\iota^2(1+k_\iota+k_{S_\iota})}, k_{S_\iota}\mu_\iota\right). \tag{12}$$

which, similarly to (8), is expressed in terms of fully convergent special functions with extensively studied properties.

IV. Numerical Results

Fig. 2 provides plots of the theoretical PDFs of the in-phase and quadrature components along with respective results of simulations for an example TSM fading scenario. It should be noted that for all examples presented in this section, the transition ratios A_0 and A_1, have been conveniently chosen to yield specific values of p_L, p_Q and p_N. For illustrative purposes, ϖ is considered to be time-invariant for all examples presented in this section. In this example the LoS state occurs most often with $p_L = 0.4$, a strong dominant component exists such that $k_L = 15$, which suffers from negligible shadowing characterized by $k_{SL} = 10$, and $\varpi_L = \pi/2$ rad. The QLoS state occurs between that of the LoS and NLoS states with a probability of $p_Q = 0.3$, it has a weaker dominant component compared to the LoS state with $k_Q = 5$, moderate shadowing with, $k_{SQ} = 1$, and $\varpi_Q = -\pi/2$ rad. Lastly, the NLoS state has a probability of occurrence of $p_N = 0.3$, a weak dominant component exists that suffers severe shadowing resulting in $k_N = 0.2$, $k_{SN} = 0.15$, and $\varpi_N = 0$ rad.

It is also noted that for all states $\bar{r}_\iota = 1$. The figure shows that the PDFs of the in-phase and quadrature components of the complex received signal of the TSM can be vastly different even when experiencing the same fading conditions. For instance, the in-phase component appears to be unimodal, whilst the quadrature component is not. The effect p_ι has on the PDF of the TSM received signal envelope is now examined in Fig. 2, using the same fading conditions which provided the results in Fig. 3 with p_ι now varying. In this example, the LoS state resembles Rician fading due to the strong dominant component and the weak shadowing, whilst the NLoS state resembles Rayleigh fading.

V. Conclusion

In this paper, for the first time, we have unified LoS, QLoS and NLoS signal propagation under the umbrella of the proposed Three State Model. To this end, the TSM has been shown to have a strong physical motivation in relation to realistic scenarios encountered in practical communication scenarios. More precisely, within each of its constituent states, fading is assumed to follow that described by the Rician fading model, with one significant departure. That is the optional presence of a dominant component, which may or may not be shadowed. The shadowing in this case is assumed to follow a separate Rician distribution, allowing the TSM to be fully defined in terms of underlying Gaussian random variables. This has the benefit, that simulation of the TSM is relatively straightforward, further advocating its adoption as a comprehensive fading model. We have also derived important first-

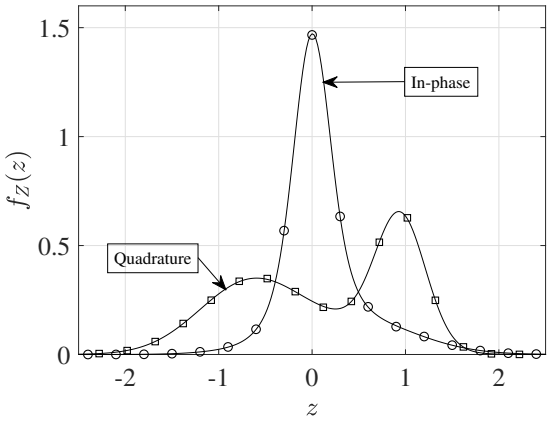

Fig. 3: The in-phase and quadrature PDFs of the TSM (lines) and corresponding simulation results (shapes).

order statistics necessary for a complete characterization of the complex received signal envelope. A number of examples have been provided for these statistics alongside respective simulated results to demonstrate their validity.

Future work related to the proposed model is concerned with the derivation of additional first-order and second-order statistics of the proposed fading model, including the PDFs of the joint envelope-phase, phase and received signal envelope as well as the complex ACF, which will be of particular importance in understanding and simulating its time correlation properties. Also, the properties and overall suitability of the proposed fading model will be experimentally quantified in the context of realistic communication scenarios in emergent technologies such as off-body communications.

REFERENCES

[1] A. F. Molisch, *Wireless Communications*, 2nd ed. Hoboken, NJ, USA: Wiley, 2011.

[2] T. S. Rappaport, *Wireless Communications: Principles and Practice*, 2nd ed. Upper Saddle River, NJ, USA: Prentice Hall, 2002.

[3] S. J. Ambroziak, L. M. Correia, R. J. Katulski, M. Mackowiak, C. Oliveira, J. Sadowski, and K. Turbic, "An off-body channel model for body area networks in indoor environments," *IEEE Trans. Antennas Propag.*, vol. 64, no. 9, pp. 4022–4035, Sep. 2016.

[4] M. Boban, T. Vinhoza, M. Ferreira, J. Barros, and O. K. Tonguz, "Impact of vehicles as obstacles in vehicular ad hoc networks," *IEEE J. Sel. Area Comm.*, vol. 29, no. 1, pp. 15–28, Jan. 2011.

[5] K. Guan, D. He, B. Ai, D. W. Matolak, Q. Wang, Z. Zhong, and T. Kürner, "5-GHz obstructed vehicle-to-vehicle channel characterization for internet of intelligent vehicles," *IEEE Internet Things J.*, vol. 6, no. 1, pp. 100–110, Feb. 2019.

[6] C.-L. Cheng and A. Zajić, "Characterization of propagation phenomena relevant for 300 GHz wireless data center links," *IEEE Trans. Antennas Propag.*, vol. 68, no. 2, pp. 1074–1087, Feb. 2020.

[7] E. R. Pelet, J. E. Salt, and G. Wells, "Effect of wind on foliage obstructed line-of-sight channel at 2.5 GHz," *IEEE Trans. Broadcast.*, vol. 50, no. 3, pp. 224–232, Sep. 2004.

[8] E. P. Moraes, J. Covolan, M. Buffalo, and L. R. Maciel, "WiMAX near LOS measurements and comparison with propagation models," in *Proc. 3rd Eur. Conf. Antennas Propag. (EuCAP)*, Mar. 2009, pp. 1–4.

[9] S. O. Rice, "Statistical properties of a sine wave plus random noise," *Bell Sys. Tech.*, vol. 27, no. 1, pp. 109–157, Jan. 1948.

[10] A. Abdi, W. C. Lau, M. S. Alouini, and M. Kaveh, "A new simple model for land mobile satellite channels: first- and second-order statistics," *IEEE Trans. Wireless Commun.*, vol. 2, no. 3, pp. 519–528, May 2003.

[11] R. F. Harrington, *Field Computation by Moment Methods*. New York, NY, USA: Wiley, 1993.

[12] J. M. Jin, *The Finite Element Method in Electromagnetics*, 2nd ed. New York, NY, USA: Wiley, 2002.

[13] A. Taflove and S. C. Hagness, *Computational Electrodynamics: The Finite-Difference Time-Domain Method*, 3rd ed. Norwood, MA, USA: Artech House, 2005.

[14] S. L. Cotton and W. G. Scanlon, "Characterization and Modeling of the Indoor Radio Channel at 868 MHz for a Mobile Bodyworn Wireless Personal Area Network," *IEEE Antennas Wireless Propag. Lett.*, vol. 6, pp. 51–55, 2007.

[15] S. L. Cotton, G. A. Conway, and W. G. Scanlon, "A time-domain approach to the analysis and modeling of on-body propagation characteristics using synchronized measurements at 2.45 GHz," *IEEE Trans. Antennas Propag.*, vol. 57, no. 4, pp. 943–955, Apr. 2009.

[16] S. L. Cotton, "A statistical model for shadowed body-centric communications channels: Theory and validation," *IEEE Trans. Antennas Propag.*, vol. 62, no. 3, pp. 1416–1424, Mar. 2014.

[17] N. Bhargav, S. L. Cotton, and D. E. Simmons, "Secrecy capacity analysis over κ–μ fading channels: Theory and applications," *IEEE Trans. Commun.*, vol. 64, no. 7, pp. 3011–3024, Jul. 2016.

[18] S. L. Cotton, "Human body shadowing in cellular device-to-device communications: channel modeling using the shadowed κ-μ fading model," *IEEE J. Sel. Areas Commun.*, vol. 33, no. 1, pp. 111–119, Jan. 2015.

[19] I. Sen and D. W. Matolak, "Vehicle–vehicle channel models for the 5-GHz band," *IEEE Trans. Intell. Transp. Syst.*, vol. 9, no. 2, pp. 235–245, Jun. 2008.

[20] D. W. Matolak and J. Frolik, "Worse-than-Rayleigh fading: Experimental results and theoretical models," *IEEE Commun. Mag.*, vol. 49, no. 4, pp. 140–146, Apr. 2011.

[21] W. Khawaja, I. Guvenc, and D. Matolak, "UWB channel sounding and modeling for UAV air-to-ground propagation channels," in *Proc. IEEE Global Commun. Conf. (GLOBECOM)*, Dec. 2016, pp. 1–7.

[22] Z. Qiu, X. Chu, C. Calvo-Ramirez, C. Briso, and X. Yin, "Low altitude UAV air-to-ground channel measurement and modeling in semiurban environments," *Wireless Commun. and Mobile Computing*, vol. 2017, Nov. 2017.

[23] J. M. Romero-Jerez, F. J. Lopez-Martinez, J. F. Paris, and A. J. Goldsmith, "The fluctuating two-ray fading model: Statistical characterization and performance analysis," *IEEE Trans. Wireless Commun.*, vol. 16, no. 7, pp. 4420–4432, Jul. 2017.

[24] U. Fernandez-Plazaola, J. Lopez-Fernandez, J. F. Paris, and E. Martos-Naya, "A tractable fading channel model with two-sided bimodality," *IEEE Access*, vol. 7, pp. 99 928–99 936, 2019.

[25] E. N. Gilbert, "Capacity of a burst-noise channel," *Bell Syst. Tech. J.*, vol. 39, no. 5, pp. 1253–1265, Sep. 1960.

[26] E. O. Elliott, "Estimates of error rates for codes on burst-noise channels," *Bell Syst. Tech. J.*, vol. 42, no. 5, pp. 1977–1997, Sep. 1963.

[27] H. S. Wang and N. Moayeri, "Finite-state Markov channel-a useful model for radio communication channels," *IEEE Trans. Veh. Technol.*, vol. 44, no. 1, pp. 163–171, Feb. 1995.

[28] Q. Zhang and S. Kassam, "Finite-state Markov model for Rayleigh fading channels," *IEEE Trans. Commun.*, vol. 47, no. 11, pp. 1688–1692, Nov. 1999.

[29] A. Abdi, J. A. Barger, and M. Kaveh, "A parametric model for the distribution of the angle of arrival and the associated correlation function and power spectrum at the mobile station," *IEEE Trans. Veh. Technol.*, vol. 51, no. 3, pp. 425–434, May 2002.

[30] M. D. Yacoub, *Foundations of Mobile Radio Engineering*, 1st ed. Boca Raton, USA: CRC Press, 1993.

[31] T. Aulin, "A modified model for the fading signal at a mobile radio channel," *IEEE Trans. Veh. Technol.*, vol. 28, no. 3, pp. 182–203, Aug. 1979.

[32] G. L. Stüber, *Principles of Mobile Communication*, 3rd ed. Springer, 2011.

[33] I. S. Gradshteyn and I. M. Ryzhik, *Table of Integrals, Series, and Products*, 7th ed. San Diego, CA, USA: Academic Press, 2007.

[34] J. G. Proakis, *Digital Communications*, 4th ed. New York: McGraw-Hill, 2001.

[35] J. W. Browning, S. L. Cotton, D. Morales-Jimenez, and F. J. Lopez-Martinez, "The Rician complex envelope under line of sight shadowing," *IEEE Commun. Lett.*, vol. 23, no. 12, pp. 2182–2186, Dec. 2019.

[36] "Wolfram Research, Inc." accessed on 03/25/2019. [Online]. Available: http://functions.wolfram.com/

[37] H. M. Srivastava and P. W. Karlsson, *Multiple Gaussian Hypergeometric Series*. John Wiley & Sons, 1985.

[38] N. Simmons, C. R. N. D. Silva, S. L. Cotton, P. C. Sofotasios, S. K. Yoo, and M. D. Yacoub, "On shadowing the κ-μ fading model," *IEEE Access*, vol. 8, pp. 120 513–120 536, 2020.